Massive growth of a fibrous gas hydrate from surface macropores of an activated carbon

Saphir Venet, Hannelore Derluyn, Fabrice Guerton, Peter Moonen, Daniel Broseta, Ross Brown

Massive growth of a fibrous gas hydrate from surface macropores of an activated carbon

2022-09-30 14:16:55+02:00

Saphir Venet[a], Hannelore Derluyn[b], Fabrice Guerton[c], Peter Moonen[b], Daniel Broseta[a], Ross Brown[d]

[a]*Universite de Pau et des Pays de l'Adour E2S UPPA CNRS TotalEnergies LFCR Pau France*
[b]*Universite de Pau et des Pays de l'Adour E2S UPPA CNRS TotalEnergies DMEX Pau France*
[c]*Universite de Pau et des Pays de l'Adour E2S UPPA CNRS TotalEnergies IPRA Pau France*
[d]*Universite de Pau et des Pays de l'Adour E2S UPPA CNRS IPREM Pau France*

Preprint submitted to Elsevier *Friday 30th September, 2022*

1. Introduction

Some 200 years after the first preparation of gas hydrates (Sloan and Koh, 2008), they still are known to the general public mainly for the enormous deposits of methane hydrate in marine sediment and the permafrost. While many applications have been proposed, like water treatment (Mottet, B. BGH; Mallek et al., 2020) and desalination(Kang et al., 2014; Ho-Van et al., 2019; Khan et al., 2019; Hong et al., 2019; Ling et al., 231; Tanaka et al., 2021), secondary refrigeration (Ruffine et al., 2018) (as a phase-change material) and gas storage (Yang et al., 2014; Veluswamy et al., 2018; Tian et al., 2022) and separation (Liu et al., 2019; Maruyama et al., 0), none to our knowledge have reached general use. A serious difficulty is the predominant growth mode of hydrates of many water-insoluble guests. They form thin films of hydrate over guest- bulk water interfaces (then usually called crust) or ride as thin layers over a film of water between a substrate or a vessel wall and the guest (called halos (Beltrán and Servio, 2010)). These polycrystalline films rapidly become impervious as they thicken, cutting off diffusion between the guest and the host and limiting hydrate production. While mechanical stirring (Yang et al., 2014; Lv et al., 2017; Nguyen et al., 2017; Nashed et al., 2018) or use of additives such as surfactants (Kumar et al., 2015; Nguyen et al., 2017; He et al., 2019; Venet et al., 2022) may side-step or attenuate the difficulty, their associated energetic or environmental disadvantages make sustained, additive-free growth in a quiescent system a still desired goal.

Promotion of hydrates by mostly micro- or meso-porous substrates and potential hydrate storage in such materials therefore receive continued attention (Li et al., 2016; Nguyen et al., 2017, 2020; Mallek et al., 2020, 2022) . However, the experimentally inconvenient equilibrium temperatures and presures of most hydrates make their location in porous materials more often assumed or inferred than directly observed. For example, remarkable amounts of methane hydrate obtained with activated carbons (Casco et al., 2014, 2015; Borchardt et al., 2016; Cuadrado-Collados et al., 2018; Casco et al., 2019; Cuadrado-Collados et al., 2020a,b), were inferred to lie outside the substrate (Casco et al., 2021), and similarly for porous silica (Zhou et al., 2005, 2006; Zhang et al., 2014). More recently, methane and carbon dioxide hydrates were inferred in meso- or macropores or interstitials of metal oxide frameworks (Denning et al., 2020, 2021a,b). Reports of directly observed morphology indicate hydrate crust or halo over the outer surface of the porous material, which is undesirable, *e.g.* refs. Babu et al. (2013); Zhang et al. (2020).

Hydrate fibres are sometimes observed as an unusual, minor morphology, growing into the guest phase on interfacial crust or on halos (Servio and Englezos, 2004; Zhang et al., 2020, 2021; Le et al., 2021). Figure 1a,b shows examples. Such

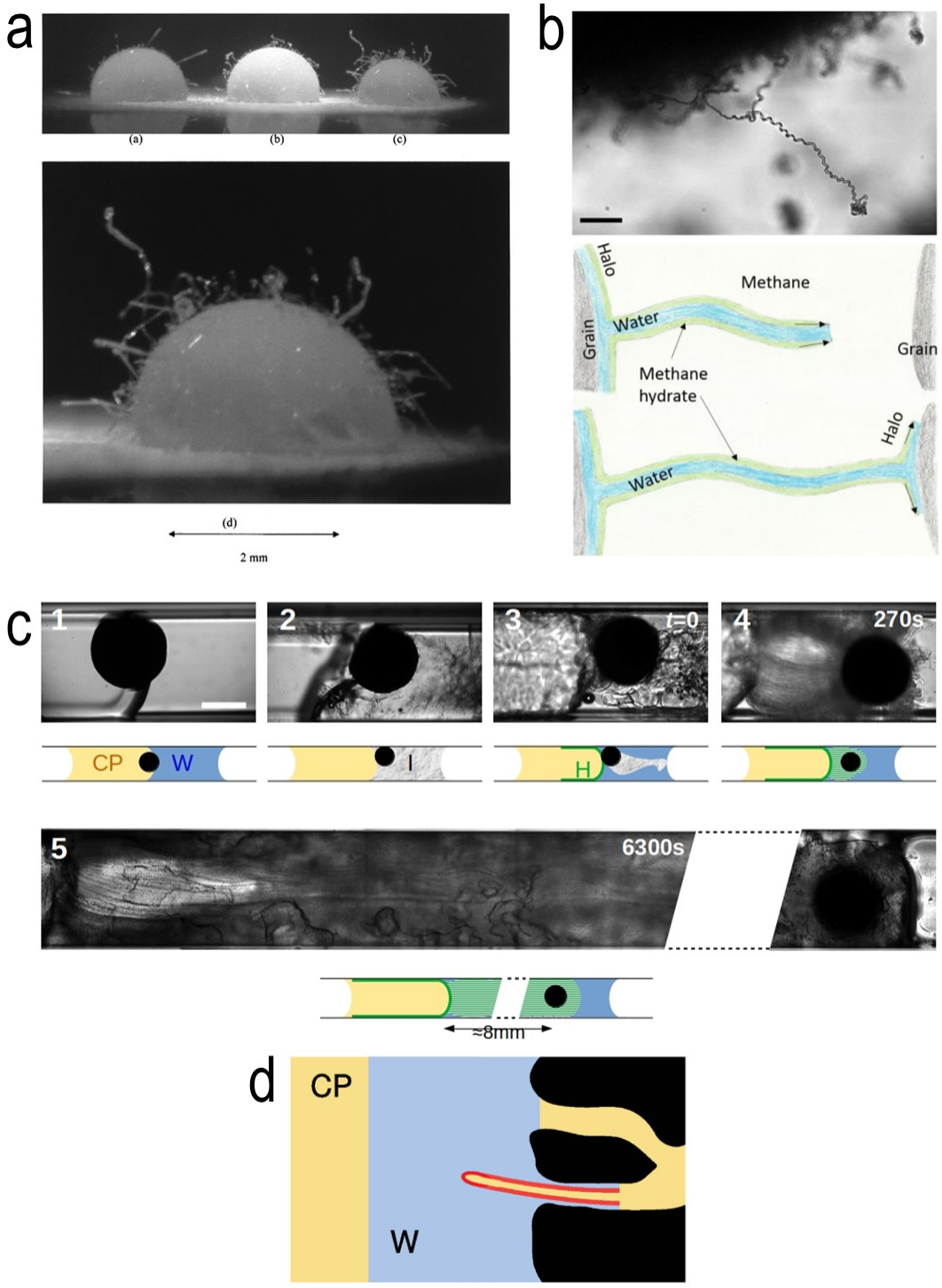

Figure 1: **Comparison of the novel fibrous hydrate morphology in ref. Venet et al. (2021) with individual filaments on crusts and halos** Individual fibres of methane hydrate growing into the guest phase on the crust over: ***(a)*** a sessile droplet (Servio and Englezos, 2004), or ***(b)*** on sand particles (Le et al., 2021), scale bar 50 μm with a schematic of growth at the fibre tip; ***(c)*** Transmission image of profuse hydrate fibres on a commercial activated carbon bead, near the interface with water in a glass capillary (Venet et al., 2021) (Activated carbon bead AC, cyclopentane CP, water W, scale bar 200 μm); ***(d)*** Cartoon of hydrate fibre formation in surface macropores deduced phenomenologically in that paper. (Activated carbon bead AC, cyclopentane CP, water W) ***N.B.* Editor: *(a,b)* Permissions required.**

fibres lengthen at their tips, implying they are hollow and that water flows in them to feed crystallisation at the tip. Thus, although fibres avoid the above mass-transfer bottleneck at water-guest interfaces, by growing into the third dimension, those observed until recently were sparse and short, typically a few 100 μm.

Similar but much denser fibres, growing by a different mechanism discussed below, were observed in ref. Venet et al. (2021): profuse masses of cyclopentane hydrate fibres produced at the external surface of commercial activated carbon beads close to water-guest interfaces, figure 1c. Those fibres outgrew the sample cell, reaching ≈ 10 mm. It was surmised that they arise in surface macropores of the substrate, fed by flow of one fluid through the internal porosity of the substrate, the other being either present at the substrate surface or flowing through fibres anchored to a guest-host interface.

Here, by applying several bulk and surface characterisation techniques, we relate the porous structure of the carbon beads to the growth of hydrate fibre bundles. We characterise the porosity accessible to water and cyclopentane separately or in competition, by gravimetric analysis and beam attenuation in X-ray radiography. *In situ* video-microscopy associates hydrate fibres with $\approx 10 - 100\,\mu$m pits on the external surface of the substrate, which also appear *ex situ* in confocal reflectance and scanning electron microscopy. Aligned macropores at and just under the external surface, are revealed by computed X-ray microtomography, explaining the whalebone-like morphology of bundles of hydrate fibres in ref. Venet et al. (2021).

2. Materials and Methods

See Supplementary Notes 1–3 for full details of the experimental methods.

2.1. Materials

We used commercial activated carbon beads (Kureha, A-BAC SP), cyclopentane (Aldrich) and deionised water (Purelab Classic System, 18 MΩcm^{-1}). X-ray data were acquired in 10 cm-long square borosilicate glass capillary sample cells (VitroTubes, CMScientific, 500/700 μm internal/external sides). A silica photometric absorption cell, path length 2 mm was used for optical microscopy (Hellma model 110-2-40).

2.2. Methods

Sample cells were mounted in home made temperature control stages on the tomograph (Zeiss Versa 510) or the inverted optical microscope (Nikon, Ti-Eclipse, x20 ELWD objective, Hamamatsu Orca 4.0 camera). Cyclopentane hydrate formed from the melt-water (0.5 °C) after quenching to form ice (≈ -20 °C).

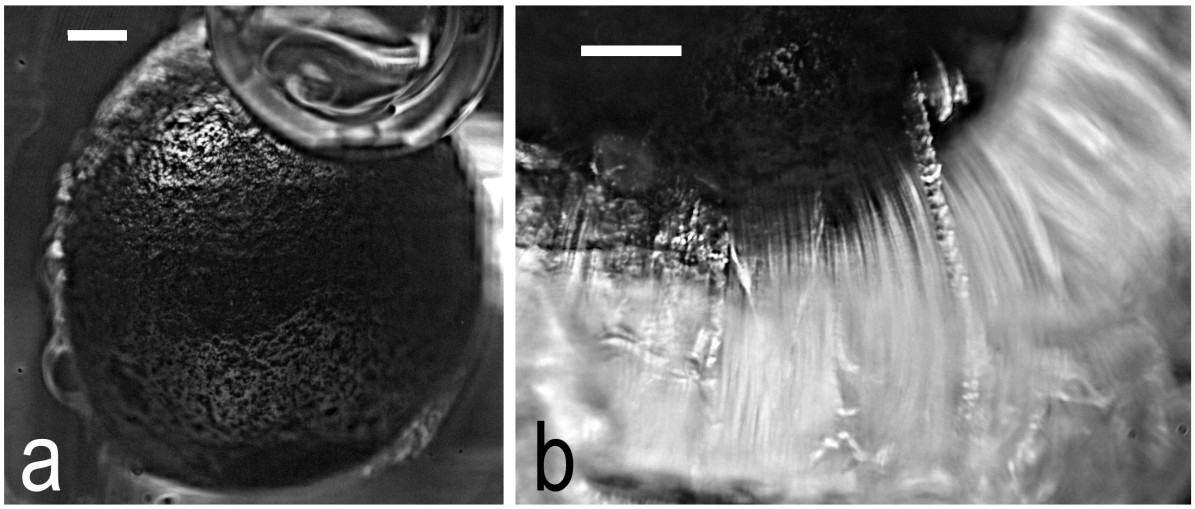

Figure 2: **Cyclopentane hydrate filaments arise from macropores at the external surface of an activated carbon bead** *(a)* Scattered light image of a bead (still degassing) at the cyclopentane-water interface at room temperature, showing pits ; *(b)* Cyclopentane hydrate fibres extruded from the pits into water at 0.5 °C. Scale bars: 200 μm.

3. Results

Fibres grow from their root in micron-sized pores in the external surface of the substrate

The experimental protocol closely follows ref. Venet et al. (2021), in which the porous substrate, here a commercial activated carbon bead, is brought into contact with the cyclopentane-host meniscus in a transparent cell, here a 2 mm path-length photometric absorption cell. Nucleation of the hydrate in a reasonable time in small samples for microscopy proceeds by quenching to form ice (*ca.* -20 °C), warming and nucleation of the hydrate with melt-water at 0.5 °C. A crust forms over the meniscus, prolonged on the glass under cyclopentane by a halo. Seconds later, comb or whalebone-like streamers of fused hydrate fibres emerge from the bead into the water. See ref. Venet et al. (2021) for details of several possible outcomes when the hydrate combs happen to push the bead around. That paper also showed the hydrate fibres are hollow and may sustain growth by conducting either liquid to the site of elongation. Here, we focus on the simplest case, when the bead remains astride the meniscus. Ref. Venet et al. (2021) concluded from the straightness of the fibres compared to their individual diameters, a few μm, that elongation occurs at or just beneath the bead surface, in micron-sized pores.

Improved illumination and resolution in figure 2a show the bead surface comprises darker, $\approx$ 10–50 μm diameter pores or pits appearing in a smoother ground.

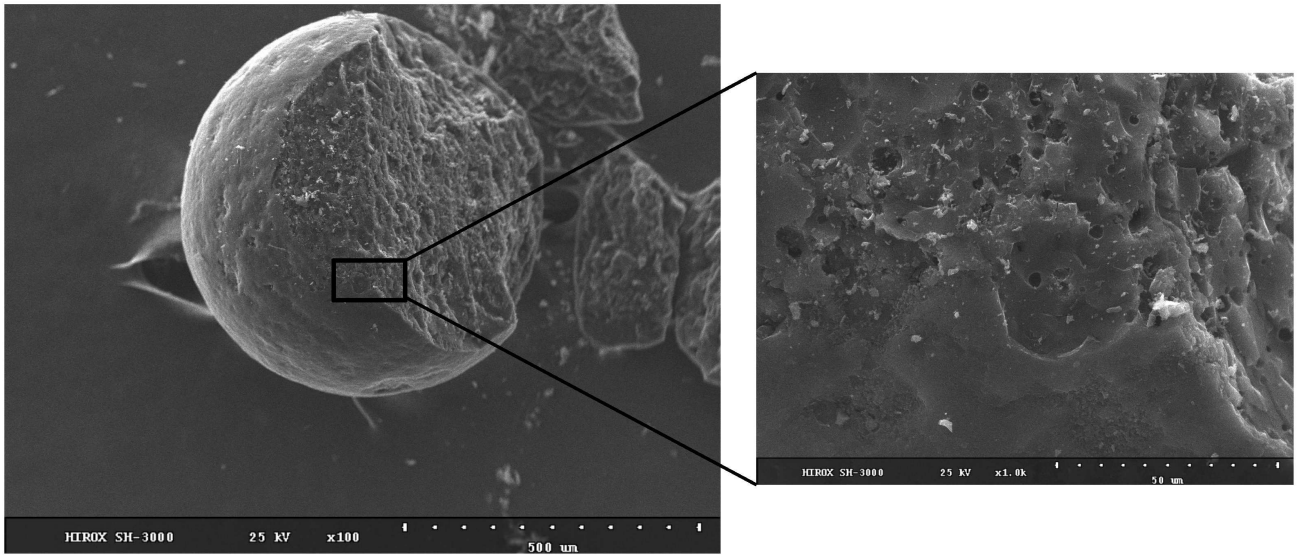

Figure 3: **Scanning electron micrographs**
Scanning electron micrographs of an activated carbon bead, showing surface pits and pores connected to the bead interior.

Part b and *in situ* Supplementary Video 1 indeed show the hydrate growing from these pits. Some pores produce no fibres; some bleb strings of hydrate lumps (*cf.* the video), which could mean that one component does not reach the growth site quickly enough, most likely cyclopentane, which has to flow through the porous substrate. But most fibres are continuously extruded from the surface pits. *Ex situ* scanning electron microscopy and confocal reflectance microscopy, figures 3 and 4 show representative samples of the topography of the bead surface in more detail. The pits responsible for hydrate fibres are about 20 μm deep and wide.

Wetting and fluid exchange in the beads

Wetting Ref. Venet et al. (2021) concluded phenomenologically that fibres arise at water-guest interfaces in surface macropores- deep enough below the surface to mould the fibre, but not too deep, since the fibres emerging from the surface are straight. X-ray imaging is appealing, and is widely applied to gas hydrate morphology (Ma et al., 2019). Unfortunately, the rate of formation of hydrate here excludes *in situ* laboratory X-ray tomography. Plain radiography shows fibres outside the bead, similar to those in figure 1, see Supplementary Figure 1. Improving the signal to noise and or the contrast between the phases

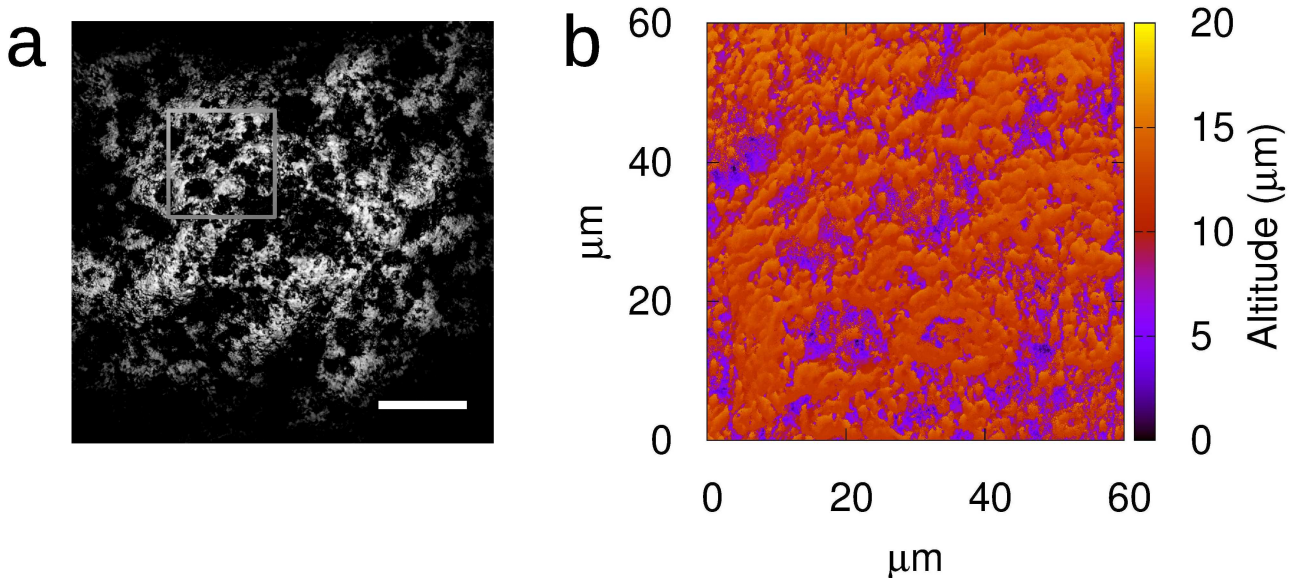

Figure 4: **Macroscopic surface pores**
a Confocal reflectance image of an activated carbon bead on a glass cover-slip. Fringes otherwise due to interference of light reflected from the bead surface and the coverslip are suppressed by use of immersion oil matching the glass. Scale bar: 50 μm; **b** Maximum projection topographic map of the boxed area in a, derived from a stack of images with vertical step 0.45 μm.

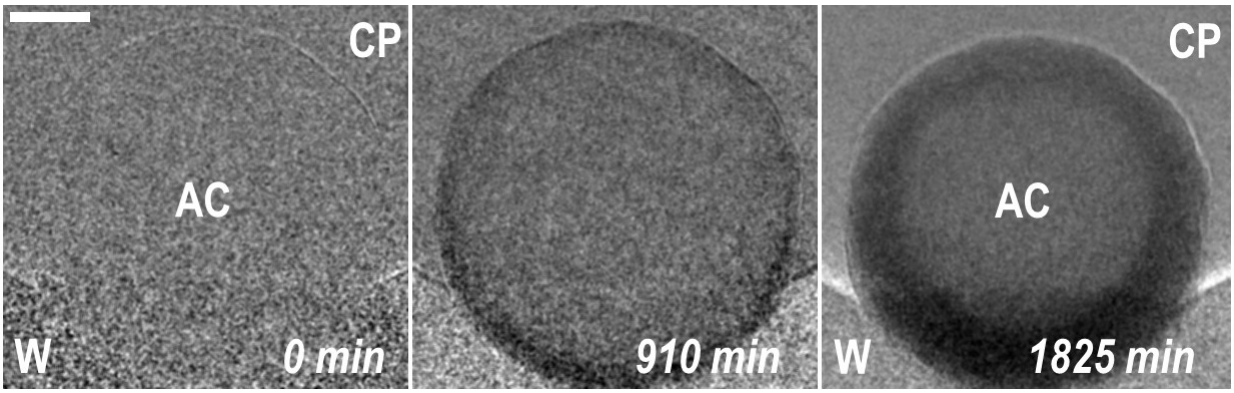

Figure 5: **Partial replacement of cyclopentane by water in subsurface porosity** Sequence of X-ray images of a cyclopentane-filled bead floating on a water-cyclopentane meniscus in a vertical glass capillary (time in min from contact with the meniscus). The optical density traces partial invasion of the peripheral porosity of the bead. Scale bar: 100 μm

would be possible with a synchrotron source.

However, the existence of the above interfaces depends on wettability. The wettability of activated carbons is complex. Here, as received beads deposited on either free standing liquid degas and sink, albeit faster for cyclopentane (seconds) than for water (> 1 h), and in minutes, cyclopentane displaces water from water-filled beads pushed into the oil in a horizontal capillary (Supplementary Figure 1). Thus cyclopentane preferentially wets the beads. Although it cannot be shown that different pores have different surface properties, the wettability thus appears mixed, with a preference for cyclopentane, but water able to wet at least partly the subsurface.

Fluid exchange in the substrate Uneven hydrate growth over the bead surface, *e.g.* in figure 2b, implies a role for structures larger than the micro- or meso-porosity commonly determined by gas adsorption porometry. The microporosity of the beads is known, 0.56 μm ^{3}g^{-1} (Zhu et al., 2004; Kureha Corporation, 2020), but our operating conditions and time scales are rather different from those prevailing in gas-adsorption porometry, which furthermore says nothing about the replacement of one fluid by another. Therefore, we deduce the accessible volume fractions of the different phases and their competition by a combination of gravimetric methods and X-ray imaging.

The beads are approximately spherical, see Supplementary Figure 3. The apparent density of the beads, ρ_B, was therefore determined by weighing a sample, photographing them spread on a cover slip and converting the areas of the disks to

volumes, assuming perfect sphericity:

$$\rho_{\mathrm{B}} = \frac{3\sqrt{\pi}M}{4\sum_i S_i^{3/2}} \quad , \tag{1}$$

where M is the mass of the sample and S_i is the surface occupied by the i^{th} bead, determined by image segmentation and particle counting (Schindelin et al., 2012; Schneider and W. S. Rasband, 2012). We deduce an apparent density of the as received beads (including internal voids and physisorbed water) $\rho_{\mathrm{app}} = 0.96\,\mathrm{gcm}^{-3}$, in good agreement with the relation $\rho_{\mathrm{fill}} = (1-v)\rho_{\mathrm{app}}$, where $\rho_{\mathrm{fill}} = 0.6\,\mathrm{gcm}^{-3}$ is the fill density (Kureha Corporation, 2020), *i.e.* including interstitials, and $v = 0.36$ is the smallest interstitial volume fraction for random packed uniform spheres. After drying the sample overnight in an oven at 100 °C, and re-weighing, we find an apparent density of the dry beads (with voids) $0.85\,\mathrm{gcm}^{-3}$, implying that physisorbed water occupies a volume fraction $\phi_{\mathrm{W}} = 0.11$.

Next we determine the volume accessible to cyclopentane in the as received (and used) beads, by following the evaporation of excess cyclopentane from a sample of beads soaked in a beaker on the laboratory balance. Initial fast loss of mass due to evaporation of the free liquid crosses over to a slower rate of loss when all the excess has evaporated (Supplementary Figure 4), from which we deduce the mass of adsorbed cyclopentane and the cyclopentane volume fraction, $\phi_{\mathrm{CP}} = 0.46$ and the skeleton volume fraction, $\phi_{\mathrm{skel}} = 1 - \phi_{\mathrm{CP}} - \phi_{\mathrm{W}} = 1 - 0.46 - 0.11 = 0.43$ and skeleton density $\rho_{\mathrm{C}} = 1.98\,\mathrm{gcm}^{-3}$ (similar to graphite and to the value determined in ref. Zhu et al. (2004)), assuming that cyclopentane-adsorption has exhausted the available voids. We expect ϕ_{CP} is slightly overestimated due to residual liquid on the outer surface.

The porous volume accessible to either water or cyclopentane under the conditions of our experiments, particularly timescale, can be determined alternatively by comparing X-ray radiographs of dry and imbibed beads with models of the optical density as a function of net composition including liquid-filled voids, *cf.* figure 6a,b. Fitting the thickness of fluid along the line of site determines the volume fraction occupied in the bead, see SI section 1.6.

As a test of consistency, we first determine the amount of physisorbed water in as received beads, by setting $\rho_{\mathrm{C}} = 0.85$ as for the dry beads, and comparing the computed and experimental X-ray cross-sections (black points and line in figure 6b). The discrepancy can be removed by assuming a volume fraction $\phi_{\mathrm{W}} = 0.13$ of physisorbed water, in fair agreement with the value deduced gravimetrically.

The same method is applied in figure 6b to another bead, degassed in cyclopen-

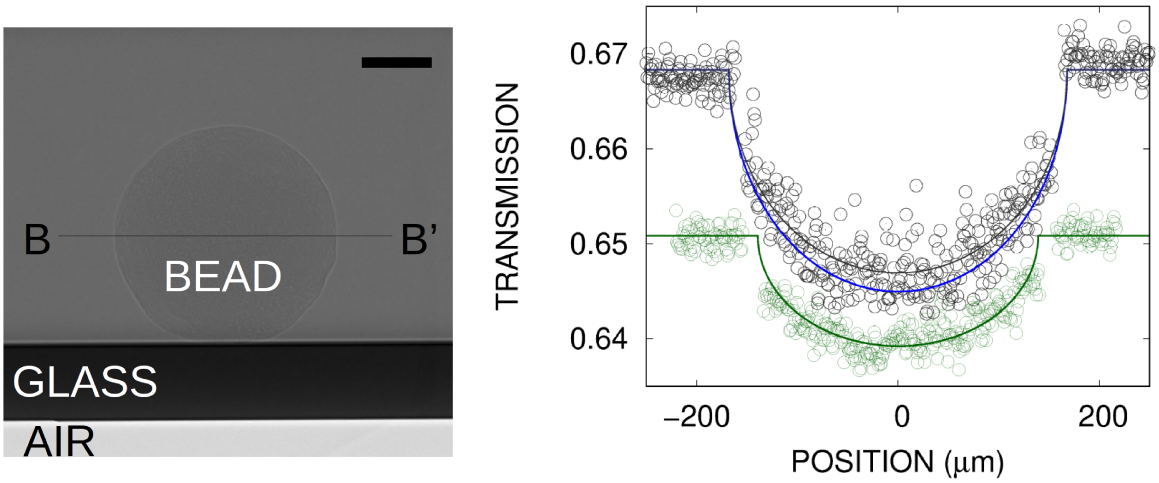

Figure 6: **Fluid content deduced from X-ray optical density**
a X-ray image (transmission) of an as-received bead loaded into a glass capillary; **b** 13 % vol. adsorbed water revealed by comparing transmission data along line BB′ (black squares) to simulations with and without water (thick blue/thin black lines). Green data and line for a different bead show additional 38 % average occupation by the guest phase on soaking in cyclopentane. Scale bar: **a**, 100 μm.

tane, holding $\rho_C = 0.85$ and $\phi_W = 0.13$ constant and adjusting ϕ_{CP} and the radius and centre of the bead, the green data and adjusted line in figure 6b. We find $\phi_{CP} = 0.38$, confirming that the gravimetric estimation of ϕ_{CP} (0.46) is overestimated. The red circle in Supplementary Figure 2 corresponds to displacement of this volume of water in a water-filled bead in cyclopentane, qualitatively consistent with the extent of the sessile droplets and supporting the assumption that cyclopentane replaces nearly all water in the bead. X-rays taken over a period of hours show that a cyclopentane-filled bead at a horizontal interface slowly adsorbs water, particularly the periphery, see figure 5 and video 2. In general both water and cyclopentane may be present in the bead sub-surface where hydrate is formed.

Origin of hydrate combs

Tomographic slices, *e.g.* figure 7 show three kinds of porosity. Round pores up to $\approx 10\,\mu$m in diameter are distributed throughout the bead. Irregular cracks $\approx 1-2\,\mu$m wide run through all the volume, connecting many pores to one another or to the surface. Additional, smaller pores, $\approx 3\,\mu$m across, also closer spaced ($< 5\,\mu$m) are found to a depth $\approx 20\,\%$ of the radius, corresponding to the depth to which water imbibes the beads in figure 5. These smaller pores line up

in circumferential bands, emerging over $\approx 50\,\%$ of the external bead surface (in the yz plane in figure 7b,c), see also the scanning electron micrographs, figure 3. Such alignments would explain the comb-like aspect of the hydrate, while the internal, connected porosity may facilitate conveyance of the guest to the sites of fibre growth.

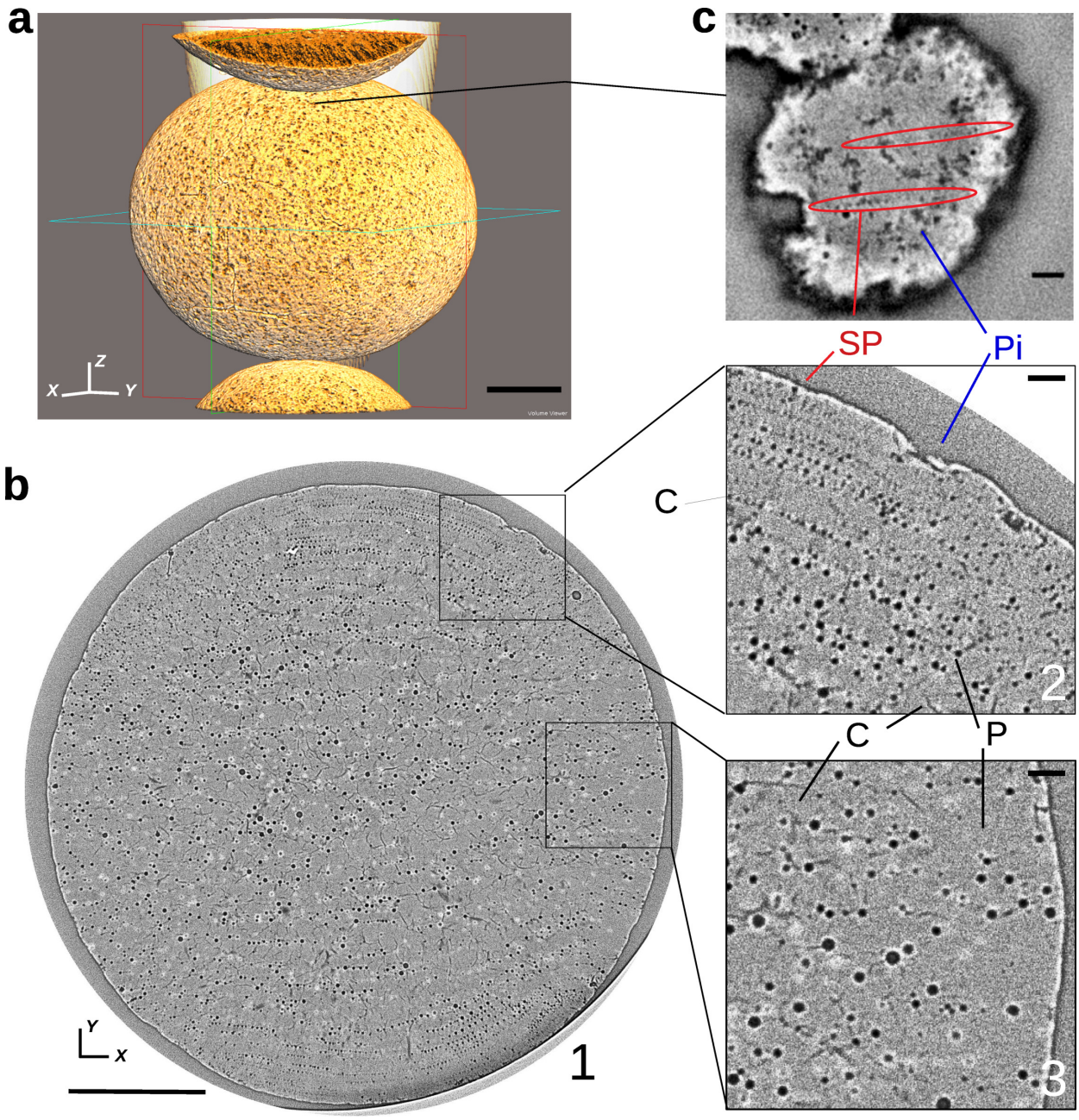

Figure 7: **Well developed and connected macroporosity of the activated carbon beads**
a Low resolution overview of the surface of a bead reconstructed from computed X-ray micro-tomography, showing surface pits and cracks; **b** A central xy slice showing (insets) surface pits (Pi) and internal pores (P) connected via cracks (C). Bands of aligned $\approx 3\mu$m pores run round one circumference; **c** Lines of these pores breaking the surface (SP) are responsible for the hydrate combs, while pits and cracks produce coarser structures. Scale bars: **a**,**b** 200 μm, insets 20 μm.

Conclusion

Much recent attention was paid to porous materials as promoters of gas hydrates and specially as possible storage vessels for them, with the focus on micro- and meso-porosity, as far they might accommodate hydrate cages. To our knowledge, however, direct visual evidence is sparse and points rather to formation of the hydrate outside the porous substrates, in the classic forms of hydrate crust or halo. Ref. Venet et al. (2021) reported an unprecedented morphology of a gas hydrate, long streamers or combs of hydrate fibres, growing into water from the surface of activated carbon beads at the guest-host interface. It was surmised phenomenologically that growth occurred in macropores at or close to the surface of the beads, the role of the internal porosity being merely to feed the guest to the growth sites.

Here therefore, we applied several analytical techniques to clarify the relation between substrate structure and hydrate morphology. *In situ* high resolution optical microscopy supersedes the earlier cartoon-explanation reproduced as figure 1b. The macropores were further characterised by SEM and computed X-ray micro-tomography. Hydrate growth in the bead surface requires simultaneous presence of both the host and the guest. A remarkable network of interconnected macropores and cracks preferentially wet by cyclopentane indeed traverses the beads, through which cyclopentane may flow to sustain hydrate formation at the bead interface with water. Although tomography and X-ray radiography could not distinguish internal fluid flows on the fly, X-ray radiography during imbibition experiments shows that the beads have complex wettability, with the necessary simultaneous occupation of peripheral layers. Hydrate promotion by porous materials is usually assumed to occur inside them, making them like tiny hydrate storage warehouses. Here, the substrate behaves more like a 'lean' or 'just in time' production line, with hydrate formed near the substrate surface and extruded as fast as it is produced. Further investigations are needed to check if these observations hold for other activated carbons, and if not, what properties of the substrate control the formation of hydrate fibres.

Acknowledgements

S. V. acknowledges ISIFoR and UPPA for post-doctoral positions. We thank V. Pelerin, IPREM for the scanning electron micrographs, J. Diaz LFCR for help setting up the experiments, P. Le Mélinaire, BGH, Lacq, France, for drawing our attention to the promotion of cyclopentane hydrate by activated carbon beads and TotalEnergies for access to the X-ray micro-tomograph.

4. Bibliography

Babu, P., Yee, D., Linga, P., Palmer, A., Khoo, B.C., Tan, T.S., Rangsunvigit, P., 2013. Morphology of methane hydrate formation in porous media. Energy & Fuels 27, 3364–3372. doi:10.1021/ef4004818.

Beltrán, J.G., Servio, P., 2010. Morphological investigations of methane-hydrate films formed on a glass surface. Cryst. Growth Des. 10, 4339–4347. doi:10.1021/cg1003098.

Borchardt, L., Nickel, W., Casco, M., Senkovska, I., Bon, V., Wallacher, D., Grimm, N., Krause, S., Silvestre-Albero, J., 2016. Illuminating solid gas storage in confined spaces – methane hydrate formation in porous model carbons. Phys. Chem. Chem. Phys. 18, 20607–20614. doi:10.1039/C6CP03993F.

Casco, M.E., Grätz, S., Wallacher, D., Grimm, N., Többens, D.M., Bilo, M., Speil, N., Fröba, M., Borchardt, L., 2021. Influence of surface wettability on methane hydrate formation in hydrophilic and hydrophobic mesoporous silicas. Chemical Engineering Journal 405, 126955. doi:https://doi.org/10.1016/j.cej.2020.126955.

Casco, M.E., Martínez-Escandell, M., Gadea-Ramos, E., Kaneko, K., Silvestre-Albero, J., Rodríguez-Reinoso, F., 2015. High-pressure methane storage in porous materials: Are carbon materials in the pole position? Chem. Mater. 27, 959–964. doi:10.1021/cm5042524.

Casco, M.E., Silvestre-Albero, J., Ramírez-Cuesta, A.J., Rey, F., Jordá, J.L., Bansode, A., Urakawa, A., Peral, I., Martínez-Escandell, M., Kaneko, K., Rodríguez-Reinoso, F., 2014. Methane hydrate formation in confined nanospace can surpass nature. Nature Comm. 6, 6432. doi:DOI: 10.1038/ncomms7432.

Casco, M.E., Zhang, E., Grätz, S., Krause, S., Bon, V., Wallacher, D., Grimm, N., Többens, D.M., Hauß, T., Borchardt, L., 2019. Experimental evidence of confined methane hydrate in hydrophilic and hydrophobic model carbons. J. Phys. Chem. C 123, 24071–24079. doi:10.1021/acs.jpcc.9b06366.

Cuadrado-Collados, C., Farrando-Pérez, J., Martínez-Escandell, M., Missyul, A., Silvestre-Albero, J., 2020a. Effect of additives in the nucleation and growth of methane hydrates confined in a high-surface area activated carbon material. Chem. Eng. J. 388, 124224. doi:https://doi.org/10.1016/j.cej.2020.124224.

Cuadrado-Collados, C., Fauth, F., Such-Basañez, I., Martínez-Escandell, M., Silvestre-Albero, J., 2018. Methane hydrate formation in the confined nanospace of activated carbons in seawater environment. Microporous and Mesoporous Materials 255, 220–225. doi:https://doi.org/10.1016/j.micromeso.2017.07.047.

Cuadrado-Collados, C., Majid, A.A., Martínez-Escandell, M., Daemen, L.L., Missyul, A., Koh, C., Silvestre-Albero, J., 2020b. Freezing/melting of water in the confined nanospace of carbon materials: Effect of an external stimulus. Carbon 158, 346–355. doi:https://doi.org/10.1016/j.carbon.2019.10.081.

Denning, S., Lucero, J.M., Majid, A.A.A., Crawford, J.M., Carreon, M.A., Koh, C.A., 2021a. Porous organic cage cc3: An effective promoter for methane hydrate formation for natural gas storage. The Journal of Physical Chemistry C 125, 20512–20521. doi:10.1021/acs.jpcc.1c04657.

Denning, S., Majid, A.A., Lucero, J.M., Crawford, J.M., Carreon, M.A., Koh, C.A., 2020. Metal–organic framework hkust-1 promotes methane hydrate formation for improved gas storage capacity. ACS Applied Materials & Interfaces 12, 53510–53518. doi:10.1021/acsami.0c15675. pMID: 33186007.

Denning, S., Majid, A.A.A., Lucero, J.M., Crawford, J.M., Carreon, M.A., Koh, C.A., 2021b. Methane hydrate growth promoted by microporous zeolitic imidazolate frameworks zif-8 and zif-67 for enhanced methane storage. ACS Sustainable Chemistry & Engineering 9, 9001–9010. doi:10.1021/acssuschemeng.1c01488.

He, Y., Sun, M.T., Chen, C., Zhang, G.D., Chao, K., Lin, Y., Wang, F., 2019. Surfactant-based promotion to gas hydrate formation for energy storage. J. Mater. Chem. A 7, 21634–21661. doi:10.1039/C9TA07071K.

Ho-Van, S., Bouillot, B., Douzet, J., "Maghsoodloo Babakhani", S., Herri, J., 2019. Cyclopentane hydrates – a candidate for desalination? J. Env. Chem. Eng. 7, 103359. doi:10.1016/j.jece.2019.103359.

Hong, S., Moon, S., Lee, Y., Lee, S., Park, Y., 2019. Investigation of thermodynamic and kinetic effects of cyclopentane derivatives on CO_2 hydrates for potential application to seawater desalination. Chem. Eng. J. 363, 99 – 106. doi:https://doi.org/10.1016/j.cej.2019.01.108.

Kang, K.C., Linga, P., Park, K., Choi, S.J., Lee, J.D., 2014. Seawater desalination by gas hydrate process and removal characteristics of dissolved

ions (Na^+, K+, Mg^{2+}, Ca^{2+}, B^{3+}, Cl^-, SO_4^{2-}). Desalination 353, 84 – 90. doi:https://doi.org/10.1016/j.desal.2014.09.007.

Khan, M.N., Peters, C.J., Koh, C.A., 2019. Desalination using gas hydrates: The role of crystal nucleation, growth and separation. Desalination 468, 114049. doi:https://doi.org/10.1016/j.desal.2019.06.015.

Kumar, A., Bhattacharjee, G., Kulkarni, B.D., Kumar, R., 2015. Role of surfactants in promoting gas hydrate formation. Industrial & Engineering Chemistry Research 54, 12217–12232. doi:10.1021/acs.iecr.5b03476.

Kureha Corporation, 2020. Bead-shaped activated carbon bac. Consulted: Oct. 2020.

Le, T.X., Bornert, M., Brown, R., Aimedieu, P., Broseta, D., Chabot, B., King, A., Tang, A.M., 2021. Combining optical microscopy and x-ray computed tomography reveals novel morphologies and growth processes of methane hydrate in sand pores. Energies 14, 5672. doi:10.3390/en14185672.

Li, Z., Zhong, D.L., Lu, Y.Y., Wang, J.L., Qing, S.L., Yan, J., 2016. Enhanced separation of carbon dioxide from a co2 + ch4 gas mixture using a hybrid adsorption-hydrate formation process in the presence of coal particles. Journal of Natural Gas Science and Engineering 35, 1472 – 1479. doi:https://doi.org/10.1016/j.jngse.2016.03.081. gas Hydrates and Applications.

Ling, Z., Shi, C., Li, F., Fu, Y., Zhao, J., Dong, H., Yang, Y., Zhou, H., Wang, S., Song, Y., 231. Desalination and li^+ enrichment via formation of cyclopentane hydrate. Separation Purif. Tech. 231, 115921. doi:10.1016/j.seppur.2019.115921.

Liu, J., Wei, Y., Meng, W., Li, P.Z., Zhao, Y., Zou, R., 2019. Understanding the pathway of gas hydrate formation with porous materials for enhanced gas separation. Research doi:doi.org/10.34133/2019/3206024.

Lv, Y.N., Wang, S.S., Sun, C.Y., Gong, J., Chen, G.J., 2017. Desalination by forming hydrate from brine in cyclopentane dispersion system. Desalination 413, 217 – 222. doi:https://doi.org/10.1016/j.desal.2017.03.025.

Ma, S., Zheng, J.n., Tang, D., Li, Y., Li, Q., Lv, X., 2019. Application of x-ray computed tomography technology in gas hydrate. Energy Technology 7, 1800699. doi:https://doi.org/10.1002/ente.201800699.

Mallek, R., Miqueu, C., Jacob, M., Dicharry, C., 2022. Investigation on hydrate formation from cyclopentane-loaded porous activated carbon particles. Chemical Engineering Science 257, 117714. doi:https://doi.org/10.1016/j.ces.2022.117714.

Mallek, R., Miqueu, C., Jacob, M., Le Mélinaire, P., Dicharry, C., 2020. Effect of porous activated carbon particles soaked in cyclopentane on CP-hydrate formation in synthetic produced water. J. Water Process Eng. 38, 101660. doi:https://doi.org/10.1016/j.jwpe.2020.101660.

Maruyama, M., Kao, S., Kiyokawa, H., Takeya, S., Ohmura, R., 0. Continuous co2 separation from a n2 + co2 gas mixture using clathrate hydrate: Insights into sustainable post-combustion carbon capture. Energy & Fuels 0, null. doi:10.1021/acs.energyfuels.2c01355.

Mottet, B. BGH, . Procédés pour cristalliser des clathrates hydrates, et procédé de purification d'un liquide aqueux utilisant les clathrates hydrates ainsi cristallisés. European patent EP3153606 (2017).

Nashed, O., Partoon, B., Lal, B., Sabil, K.M., Shariff, A.M., 2018. Review the impact of nanoparticles on the thermodynamics and kinetics of gas hydrate formation. J. Nat. Gas Sci. and Eng. 55, 452 – 465. doi:https://doi.org/10.1016/j.jngse.2018.05.022.

Nguyen, N.N., Galib, M., Nguyen, A.V., 2020. Critical review on gas hydrate formation at solid surfaces and in confined spaces—why and how does interfacial regime matter? Energy & Fuels 34, 6751–6760. doi:10.1021/acs.energyfuels.0c01291.

Nguyen, N.N., Nguyen, A.V., Steel, K.M., Dang, L.X., Galib, M., 2017. Interfacial gas enrichment at hydrophobic surfaces and the origin of promotion of gas hydrate formation by hydrophobic solid particles. J. Phys. Chem. C 121, 3830–3840. doi:10.1021/acs.jpcc.6b07136.

Ruffine, L., Broseta, D., Desmedt, A., 2018. Gas Hydrates 2: Geoscience Issues and Potential Industrial Applications. Wiley-ISTE, London.

Schindelin, J., Frise, I.A.C.E., Kaynig, V., Longair, M., Pietzsch, T., Preibisch, S., Rueden, C., Saalfeld, S., Schmid, B., Tinevez, J.Y., White, D.J., Hartenstein, V., Eliceiri, K., Tomancak, P., Cardona, A., 2012. Fiji: an open-source platform for biological-image analysis. Nature Meth. 9, 676–682.

Schneider, C.A., W. S. Rasband, a.K.W.E., 2012. Nih image to imagej: 25 years of image analysis. Nature Meth. 9, 671–675. doi:10.1038/nmeth.2089.

Servio, P., Englezos, P., 2004. Morphology of methane and carbon dioxide hydrates formed from water droplets. AIChE J. 49, 269–276. doi:10.1002/aic.690490125.

Sloan, E.D., Koh, C.A., 2008. Clathrate Hydrates of Natural Gases. volume 119 of *Chemical Industries*. 3rd ed., CRC Press, Boca Raton, FL.

Tanaka, M., Tsugane, K., Suga, D., Tomura, S., Ohmura, R., Yasuda, K., 2021. Simultaneous crystallization of cyclopentane hydrate and sodium chloride for desalination and salt manufacture. ACS Sustainable Chemistry & Engineering 9, 9078–9084. doi:10.1021/acssuschemeng.1c02356.

Tian, L., Ha, L., Wang, L., Chen, G., Coulon, F., Jiang, Y., Zeng, X.Y., Zhang, R., Wu, G., 2022. Location optimization of silicon carbide foam packings in the unstirred packing trays reactor for the enhancement of solidified natural gas storage. Chemical Engineering Science 253, 117503. doi:https://doi.org/10.1016/j.ces.2022.117503.

Veluswamy, H.P., Kumar, A., Seo, Y., Lee, J.D., Linga, P., 2018. A review of solidified natural gas (SNG) technology for gas storage via clathrate hydrates. Appl. Energy 216, 262 – 285. doi:https://doi.org/10.1016/j.apenergy.2018.02.059.

Venet, S., Broseta, D., Brown, R., 2021. A novel gas hydrate morphology: Massive hollow fiber growth on a porous substrate. Crystal Growth & Design 21, 3148–3152. doi:10.1021/acs.cgd.1c00161.

Venet, S., Guerton, F., Desmedt, A., Broseta, D., 2022. Insights into the porous structure of surfactant-promoted gas hydrate. Chemical Engineering Science 248, 117193. doi:https://doi.org/10.1016/j.ces.2021.117193.

Yang, M., Song, Y., Jiang, L., Liu, W., Dou, B., Jing, W., 2014. Effects of operating mode and pressure on hydrate-based desalination and CO_2 capture in porous media. Appl. Energy 135, 504 – 511. doi:https://doi.org/10.1016/j.apenergy.2014.08.095.

Zhang, G., Liu, B., Xu, L., Zhang, R., He, Y., Wang, F., 2021. How porous surfaces influence the nucleation and growth of methane hydrates. Fuel 291, 120142. doi:https://doi.org/10.1016/j.fuel.2021.120142.

Zhang, G., Sun, M., Liu, B., Wang, F., 2020. Adsorption-induced two-way nanoconvection enhances nucleation andgrowth kinetics of methane hydrates in confined pore space. Chemical Engineering Journal 396, 125256.

Zhang, X.X., Liu, H., Sun, C.Y., Xiao, P., Liu, B., Yang, L.Y., Zhan, C.H., Wang, X.Q., Li, N., Chen, G.J., 2014. Effect of water content on separation of co2/ch4 with active carbon by adsorption–hydration hybrid method. Separation and Purification Technology 130, 132 – 140. doi:https://doi.org/10.1016/j.seppur.2014.04.028.

Zhou, L., Liu, X., Li, J., Sun, Y., Zhou, Y., 2006. Sorption/desorption equilibrium of methane in silica gel with pre-adsorption of water. Colloids and Surfaces A: Physicochemical and Engineering Aspects 273, 117–120. doi:https://doi.org/10.1016/j.colsurfa.2005.08.017.

Zhou, L., Liu, X., Sun, Y., Li, J., Zhou, Y., 2005. Methane sorption in ordered mesoporous silica sba-15 in the presence of water. The Journal of Physical Chemistry B 109, 22710–22714. doi:10.1021/jp0546002. pMID: 16853959.

Zhu, W., Groen, J., van Miltenburg, A., Kapteijn, F., Moulijn, J., 2004. Comparison of adsorption behaviour of light alkanes and alkenes on kureha activated carbon. Carbon 43, 1416–1423. doi:https://doi.org/10.1016/j.carbon.2005.01.010.